reactions

MDPI

Article

CASPT2 Study of the Unimolecular Reactions of Nitromethane—A Look at the Roaming Reactions in the Decomposition of Nitromethane: An Exergonic Route at High Temperatures

Juan Soto [1,2]

[1] Department of Physical Chemistry, Faculty of Science, University of Málaga, 29071 Málaga, Spain; soto@uma.es
[2] University Institute of Materials and Nanotechnology (IMANA), University of Málaga, 29071 Málaga, Spain

Abstract: In this work, we studied the main decomposition reactions on the ground state of nitromethane (CH_3NO_2) with the CASPT2 approach. The energetics of the main elementary reactions of the title molecule have been analyzed on the basis of Gibbs free energies obtained from standard expressions of statistical thermodynamics. In addition, we describe a mapping method (orthogonalized 3D representation) for the potential energy surfaces (PESs) by defining an orthonormal basis consisting of two R^n orthonormal vectors (n, internal degrees of freedom) that allows us to obtain a set of ordered points in the plane (vector subspace) spanned by such a basis. Geometries and harmonic frequencies of all species and orthogonalized 3D representations of the PESs have been computed with the CASPT2 approach. It is found that all of the analyzed kinetically controlled reactions of nitromethane are endergonic. For such a class of reactions, the dissociation of nitromethane into CH_3 and NO_2 is the process with the lower activation energy barrier (ΔG); that is, the C-N bond cleavage is the most favorable process. In contrast, there exists a dynamically controlled process that evolves through a roaming reaction mechanism and is an exergonic reaction at high temperatures: $CH_3NO_2 \rightarrow [CH_3\cdots NO_2]^* \rightarrow [CH_3ONO]^* \rightarrow CH_3O + NO$. The above assertions are supported by CASPT2 mappings of the potential energy surfaces (PESs) and classical trajectories obtained by "on-the fly" CASSCF molecular dynamics calculations.

Keywords: CASSCF; CASPT2; nitromethane; exergonic decomposition

Academic Editor: Dmitry Yu. Murzin

Received: 27 January 2025
Revised: 18 February 2025
Accepted: 4 March 2025
Published: 12 March 2025

Citation: Soto, J. CASPT2 Study of the Unimolecular Reactions of Nitromethane—A Look at the Roaming Reactions in the Decomposition of Nitromethane: An Exergonic Route at High Temperatures. *Reactions* **2025**, *6*, 21. https://doi.org/10.3390/reactions6010021

1. Introduction

Nitro compounds are a class of molecules that play important roles in several areas and applications, such as atmospheric chemistry, explosives, propellants, or fuels [1–3]. For this reason, the thermal and photochemical decompositions of the simplest organic nitro compound [nitromethane (CH_3NO_2)] have been extensively studied both theoretically [4–20] and experimentally [18–24], due precisely to its molecular simplicity and the applications above mentioned. There is consensus in the literature that the weakest bond in the molecule is C-N [6]. However, in spite of the structural simplicity of nitromethane, it is not clear what is the initial reaction or the key reaction step that occurs in the chemically simplest decomposition processes, for example, when it acts as an explosive without the intervention of an external reactant, or when it is decomposed in IRMPD experiments where the thermal chemistry occurs in collision-free conditions [21].

The detonation of an energetic material is a process that occurs under the stimuli of an external action that leads to a local chemical reaction, releasing an enormous amount of energy which is transformed in the internal energy of the material with the consequent local increasing of the temperature and pressure [14]. According to the definition of detonation, the initial local reaction is expected to be an elementary unimolecular process. Thus, in this context, detonation of CH_3NO_2 acting as energetic material remains a major puzzle because all of the elementary reactions of this molecule are highly endothermic (vide infra). In this work, we propose an elementary reaction that leads to an exergonic decomposition process at high temperatures that passes through the nitro–nitrite isomerization channel via a roaming reaction and ends with the dissociation of cis-methyl nitrite into CH_3O and NO. The roaming mechanism of nitromethane has been previously studied by other authors [7–9]; therefore, we assume, as a starting hypothesis, that this process takes place in the decomposition mechanism. For the sake of completeness, all of the elementary reactions of nitromethane decomposition have been studied with the CASPT2 approximation.

A roaming reaction is a class of unimolecular reaction that was reported relatively recently [25]. Roaming reactions occur at the near-dissociation limit of the molecule where radical products are almost formed; that is, when the fragments are separated to 3–4 Å, then roaming reorientation of the fragments becomes feasible, as the kinetic energy is low and, consequently, the angular forces may be comparable to the radial forces; in other words, roaming rotation of the fragments is almost a free energy process. This effect may allow the system to access a distinct reactive domain with respect to dissociation, such as abstraction or isomerization, with the consequent formation of unexpected highly vibrationally excited products [19,26]. Roaming reactions may be considered a special case of those reactions that are dynamically controlled and deviate from the minimum energy path or intrinsic reaction coordinate [27–30] and are now widely accepted as a nearly universal aspect of chemical reactivity that could make a significant contribution to product branching in unimolecular reactions [30–36].

2. Methods of Calculation

The multi-configurational calculations have been carried out with the complete active space self-consistent field (CASSCF) [37–43] method and the multi-state second-order perturbation (MS-CASPT2) approach [44,45], as implemented in the MOLCAS 8.4 and OpenMOLCAS 22.06 programs [46–49]. Extended relativistic ANO-RCC basis sets [50,51] have been used throughout this work by applying the contraction scheme [C,N,O]/[H]: [4*s*3*p*2*d*1*f*]/[3*s*2*p*1*d*]. The IPEA empirical correction has been fixed at 0.25 in all of the MS-CASPT2 calculations, equally, and to avoid the inclusion of intruder states in such calculations, an imaginary shift set to 0.1 has been applied.

All geometry optimizations have been performed with both CASSCF and CASPT2 methods. The characterization of all the species as a minimum or transition state has been conducted by means of frequency calculations, analytically for CASSCF calculations and numerically for the CASPT2 ones. In addition, the Møller–Plesset (MP2) [52] and DFT/M062X [53] methods have been applied as they are implemented in GAUSSIAN-16 [54], in conjunction with def2-TZVPP basis sets [55,56].

The selection of the active space to study the reactions of nitro–nitrite derivatives (X-NO_2; X=NO) consists of 14 electrons distributed in 11 orbitals [57–62], or 16 electrons and 13 orbitals when proton migration is under study. Molecular dynamics calculations at the CASSCF level were performed with the velocity algorithm of Verlet [63,64] implemented in MOLCAS.

The analysis of molecular orbitals and molecular geometries was conducted with the programs Molden 6.9 [65] and Gabedit 2.5.0 [66]. The analysis of vibrational normal modes was performed with the MacMolplt V7.6 program [67].

Construction of the 1D potential energy curves (PECs) was performed by applying a linear interpolation method that uses the full space of non-redundant internal coordinates [68–72].

Mapping of 2D Potential Energy Surfaces

The mapping of the 2D potential energy surface of a reaction was sketched out in a previous work [73]. Here, we describe the procedure in detail (Figure 1). First of all, to start the mapping, three points (geometrical configurations) are required for defining the reaction domain; such points usually content critical points of the system under study, e.g., minima, transition states, surface crossings, or a combination of them. Secondly, we define a common set of non-redundant internal coordinates ($\vec{R}_n = [r_i, \ldots, \alpha_j, \ldots, \Gamma_k, \ldots]$) for the three reference points, where $r_i's$ corresponds to internuclear distances and $\alpha_j's$ and $\Gamma_k's$ are valence bond angles and dihedral angles, respectively. Third, one of the selected points is chosen as a reference (0 in Figure 1A). Then, we built the linear interpolation vectors $\vec{R}_{01}$ and $\vec{R}_{02}$ by subtraction of the *i*, *j* non-redundant internal coordinates:

$$\vec{R}_{01} = \vec{R}_1 - \vec{R}_0 \quad (1)$$

$$\vec{R}_{02} = \vec{R}_2 - \vec{R}_0. \quad (2)$$

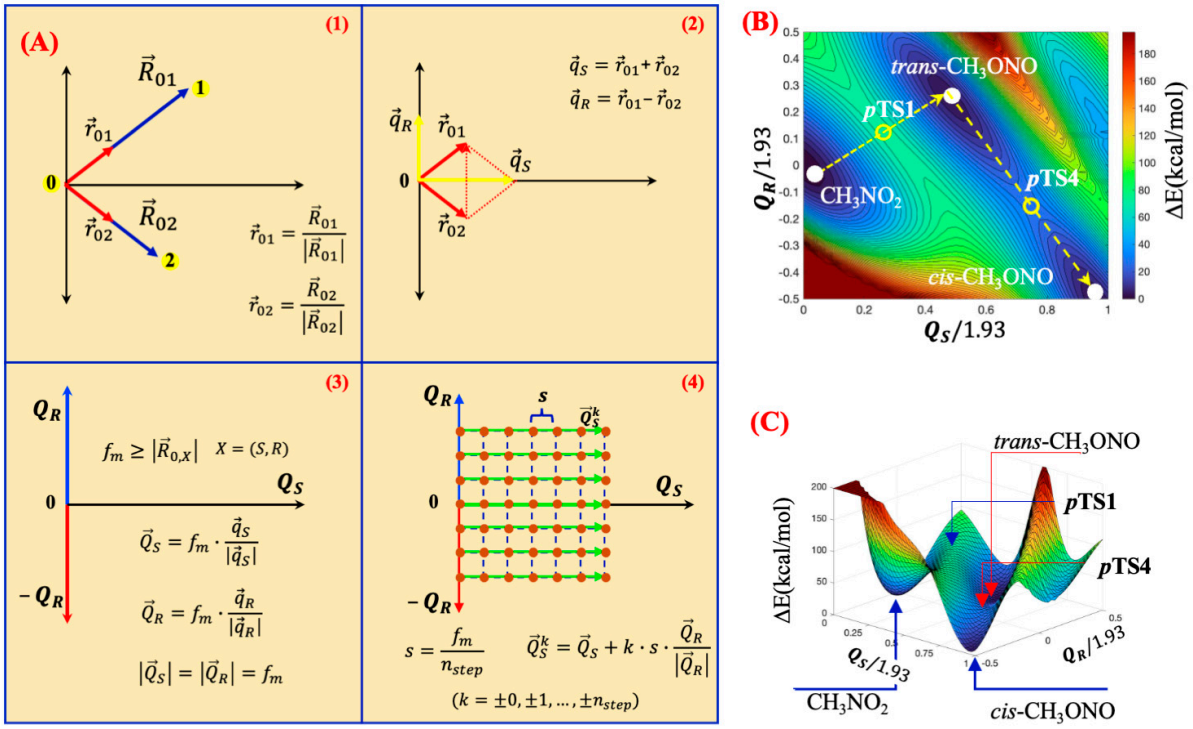

Figure 1. (**A**) Schematic representation of the orthogonalized mapping method. (**B**) CASPT2 contour plot (2D representation) of the potential energy surface (PES) connecting the system the system [nitromethane:*trans*-methylnitrite:*cis*-methylnitrite]. (**C**) CASPT2 3D representation of the PES of the same system. pTS1 and pTS4: saddle points on the PES. Grid size (41 × 41).

The coordinates of $\vec{R}_{0i}$ correspond to the following elements: non-dimensional internuclear distances $r_{0i} = (r_0 - r_i)/r_o$ (r_k internuclear distance in Å and $r_o = 1$) and the

differences between the $\alpha_{0j}'s$ and $\Gamma_{0k}'s$, respectively, which correspond to non-dimensional valence bond angle coordinates or dihedral angle coordinates of $\vec{R}_0$ and $\vec{R}_i$ in radians.

Given that we are working in internal coordinates, the relative orientation of the $\vec{R}_{01}$ and $\vec{R}_{02}$ vectors can be arbitrarily chosen. Thus, in this case, the relative orientation is selected in such a way that the bisector line of the angle **1$\hat{0}$2** is aligned with the Q_S-axis and is orthogonal to the Q_R-axis (Figure 1(A1)).

The next step is the normalization of the vectors $\vec{R}_{01}$ and $\vec{R}_{02}$:

$$\vec{r}_{01} = \vec{R}_{01} / \left|\vec{R}_{01}\right| \tag{3}$$

$$\vec{r}_{02} = \vec{R}_{02} / \left|\vec{R}_{02}\right|. \tag{4}$$

Thus, the addition and subtraction of the unit vectors $\vec{r}_{01}$ and $\vec{r}_{02}$—with equal lengths—yields vectors $\vec{v}_S$ and $\vec{v}_R$ that are mutually orthogonal and are in line with the Q_S-axis and Q_R-axis, respectively (Figure 1(A2)). Normalization of $\vec{v}_S$ and $\vec{v}_R$ yields $\vec{q}_S$ and $\vec{q}_R$ that form an orthonormal basis:

$$\vec{v}_S = \vec{r}_{01} + \vec{r}_{02}\,\vec{q}_S = \vec{v}_S / \left|\vec{v}_S\right| \tag{5}$$

$$\vec{v}_R = \vec{r}_{01} - \vec{r}_{02}\,\vec{q}_R = \vec{v}_R / \left|\vec{v}_{SR}\right|. \tag{6}$$

In order to span the configurational domains of species 1 and 2, the orthonormal vectors $\vec{q}_S$ and $\vec{q}_R$ are scaled by the norm (f_m) of the largest vector, $\vec{R}_{01}$ or $\vec{R}_{02}$. Thus, we obtain two vectors, $\vec{Q}_s$ and $\vec{Q}_R$, which are mutually orthogonal and with the same norm (Figure 1(A3)) as follows:

$$f_m \geq \left|\vec{R}_{0X}\right| X = (1\ or\ 2) \tag{7}$$

$$\vec{Q}_S = f_m \cdot \vec{q}_s \tag{8}$$

$$\vec{Q}_R = f_m \cdot \vec{q}_R \tag{9}$$

$$f_m = \left|\vec{Q}_s\right| = \left|\vec{Q}_R\right|. \tag{10}$$

Once the vectors $\vec{Q}_s$ and $\vec{Q}_R$ are built, in order to map the potential energy surface, it is necessary to select a step size s:

$$s = f_m / n_{step} \tag{11}$$

where n_{step} is an arbitrary integer number that will determine the grid size of the 2D surface. Thus, the position of any point (k, l), which represents a distortion of the reference geometry 0 ($k{\cdot}s$ times along the vector $\vec{Q}_S$ and $l{\cdot}s$ times along the vector $\vec{Q}_R$), is given by the position vector $\vec{P}_{kl}$ (Figure 1(A4)).

$$\vec{P}_{kl} = k{\cdot}s{\cdot}\vec{Q}_S / \left|\vec{Q}_S\right| + l{\cdot}s{\cdot}\vec{Q}_R / \left|\vec{Q}_R\right| \left(k, l = \pm 0, \pm 1, \ldots, \pm n_{step}\right) \tag{12}$$

In practice, we run the mapping in horizontal mode; that is, following the interpolation vector $\vec{Q}_S^{\,l}$ (Figure 1(A4)). As an example of the application of the mapping procedure described above, Figure 1B,C depicts the 2D and 3D representations of the potential energy surfaces of the ternary system [nitromethane:*trans*-methylnitrite:*cis*-methylnitrite]. The

mapping of such a system identifies two saddle points, labelled as *p*TS1 and *p*TS4, that would connect (i) nitromethane with trans-methyl nitrite and (ii) trans-methyl nitrite with cis-methyl nitrite, respectively. Thus, each one of these saddle points has been successfully used as good starting geometries to optimize the true transition states (TS1 and TS4; vide infra) for the reactions $CH_3NO_2 \rightarrow$ trans-CH_3ONO and trans-$CH_3ONO \rightarrow$ cis-CH_3ONO, respectively.

To finish this section, it must be remarked that the points used in mapping the PESs satisfy the condition of being contained in a plane because they are constructed from the basis vectors $\vec{q}_S$ and $\vec{q}_R$ that form a subspace of R^n. In contrast, the points that would be obtained by the so-called constrained optimization method would not satisfy the above condition because they would not be in the same vector subspace.

3. Results and Discussion

3.1. Unimolecular Reactions of Nitromethane and Methyl Nitrite

The elementary unimolecular reactions of nitromethane and methyl nitrite have been widely studied by many authors with a variety of theoretical approximations [4–20], mostly with single-determinantal representation for the electrons. However, given that several of the products and intermediates of the studied reactions are radical species, application of a multiconfigurational wavefunction method is demanded to avoided symmetry breaking deficiency [74], which would lead to an unappropriated description of the electronic structure of the fragments (charged fragments), for example, in studying the potential energy surfaces of the dissociation reactions (Figure S1). In this section, with the objective of showing the accuracy and reliability of the CASPT2 theory, whose reference wave function is multi-determinantal, we studied some of the main unimolecular reactions of nitromethane and methyl nitrite with such a theory (energetics, frequencies and geometries of stable species, and intermediates and transition states), and where possible, CASPT2 results are compared with experimental data [75–77] and with MP2 and DFT calculations obtained in this work. To be specific, the reactions reported are: (i) dissociation of nitromethane into methyl and nitrogen dioxide radicals; (ii) trans-methyl nitrite dissociation into methoxy and nitric oxide radicals; (iii) nitromethane dissociation into nitrosomethane and atomic oxygen; (iv) nitro–nitrite isomerization of nitromethane leading to formation of trans-methyl nitrite; (v) proton migration in nitromethane to give aci-nitromethane [$CH_2N(O)OH$]; (vi) proton migration in methyl nitrite to give formaldehyde and nitrosyl hydride (HNO); and (vii) trans–cis isomerization of methyl nitrite. The thermodynamics properties (enthalpies and Gibbs free energies) of such reactions computed with the expressions of statistical thermodynamics and obtained from three different theoretical approaches (CASPT2, MP2/HF, and DFT) are compared with experimental values in Tables 1 and 2. In general, there exists an excellent agreement between experimental and CASPT2 calculated values for the reaction enthalpies; the major source of deviation from the experimental data arises from the harmonic CASPT2 frequencies. Comparison of the dissociation and activation Gibbs energies for the tabulated reactions shows that the C-N bond cleavage is the most energetically favourable process of nitromethane. As another probe/prove of the accuracy of the CASPT2 method to deal with this kind of compound, the comparison of experimental [78–81] and calculated geometrical parameters of the species studied in this work for nitromethane, intermediates and products, is given in Supplementary Information (Tables S1–S8). Equally, in order to show that the MS-CASPT2 approach is an appropriate method to deal with dissociation reactions [82–86], the potential energy surfaces of the dissociation reactions collected in Table 1 are given in Figures S2 and S3, where it is clearly observed that every potential energy curve reaches the asymptotic limit at the dissociation region.

Table 1. Energetics (kcal/mol) of the dissociation reactions of nitromethane and methyl nitrite.

Reaction	Method	$\Delta_d G$ [a]	$\Delta_d E_e$ [b]	$\Delta_d H$ [c]	$\Delta_d H$ [d]
$CH_3NO_2(g) \rightarrow CH_3(g) + NO_2(g)$	CASPT2		65.95		
(0 K)		58.76		58.76	59.16
(298.15 K)		50.83		60.10	61.00
	MP2/HF		66.61		
(0 K)		63.71		63.71	
(298.15 K)		56.70		65.06	
	M062X		67.93		
(0 K)		60.51		60.51	
(298.15 K)		53.35		61.93	
t-$CH_3ONO(g) \rightarrow CH_3O(g)+NO(g)$	CASPT2		46.48		
(0 K)		42.60		42.60	41.11
(298.15 K)		33.13		43.99	42.32
	MP2/HF		51.10		
(0 K)		49.28		49.28	
(298.15 K)		39.79		50.69	
	M062X		42.63		
(0 K)		37.86		37.86	
(298.15 K)		28.31		39.40	
$CH_3NO_2(g) \rightarrow CH_3NO(g)+O(^3P)(g)$	CASPT2		99.53		
(0 K)		95.32		95.32	92.83
(298.15 K)		88.19		96.47	94.35
	MP2/HF		104.88		
(0 K)		100.44		100.44	
(298.15 K)		93.46		101.57	
	M062X		96.82		
(0 K)		92.53		92.53	
(298.15 K)		85.47		93.68	

[a] Gibbs free energy. [b] Electronic energy. [c] Dissociation enthalpy. [d] Dissociation enthalpy from https://atct.anl.gov/Thermochemical%20Data/ Data (accessed on 7 March 2025). Refs: [75–77].

Table 2. Energetics (kcal/mol) of the rearrangement and proton migration reactions of nitromethane and methyl nitrite.

Reaction		$\Delta_a G$ [a]	$\Delta_a E_e$ [b]	$\Delta_a H$ [c]	$\Delta_r H$ [d]	$\Delta_r H$ [d]
$CH_3NO_2(g) \xrightarrow{TS1}$ *t*-$CH_3ONO(g)$	CASPT2		69.25			
(0 K)		66.31		66.31	2.55	1.99
(298.15 K)		66.66		66.42	2.66	2.45
	MP2		71.84			
(0 K)		69.19		69.19	6.10	
(298.15 K)		69.91		69.12	5.91	
	M062X		73.15			
(0 K)		70.77		70.77	2.10	
(298.15 K)		71.33		70.77	2.44	

Table 2. *Cont.*

Reaction		$\Delta_a G$ [a]	$\Delta_a E_e$ [b]	$\Delta_a H$ [c]	$\Delta_r H$ [d]	$\Delta_r H$ [d]
$CH_3NO_2(g) \xrightarrow{TS2} CH_2N(O)OH(g)$	CASPT2		66.54			
(0 K)		63.01		63.01	12.88	
(298.15 K)		64.98		62.54	12.76	
	MP2		66.35			
(0 K)		62.86		62.86	16.32	
(298.15 K)		62.86		62.95	16.20	
	M062X		65.66			
(0 K)		62.19		62.19	12.52	
(298.15 K)		63.25		61.77	12.33	
t-$CH_3ONO(g) \xrightarrow{TS3} CH_2O(g) + HNO(g)$	CASPT2		43.80			
(0 K)		38.76		38.76	14.34	13.62 14.85
(298.15 K)		38.90		38.68	15.97	
	MP2		41.94			
(0 K)		37.69		37.69	13.42	
(298.15 K)		37.27		37.99	15.06	
	M062X		49.92			
(0 K)		45.88		45.88	14.92	
(298.15 K)		46.73		45.54	16.06	
t-$CH_3ONO(g) \xrightarrow{TS4}$ *c*-$CH_3ONO(g)$	CASPT2		12.12			
(0 K)		11.62		11.62	−0.86	−0.74
(298.15 K)		11.47		12.28	−0.60	−0.70
	MP2		11.26			
(0 K)		10.63		10.63	−1.11	
(298.15 K)		10.42		10.75	−0.94	
	M062X		10.95			
(0 K)		10.48		10.48	−1.29	
(298.15 K)		11.46		9.99	−1.66	

[a] Gibbs free energy. [b] Electronic energy. [c] Activation enthalpy. [d] Reaction enthalpy. [e] reaction enthalpy from https://atct.anl.gov/Thermochemical%20Data/ Data (accessed on 7 March 2025). Refs: [75–77].

3.2. A Look at the So-Called Loose Transition State

Two different reaction mechanisms for nitro–nitrite isomerization of nitromethane (CH_3NO_2) to methyl nitrite (CH_3ONO) have been proposed in the literature: one involves a so-called loose transition state (Figure 2a), in which the methyl and NO_2 radicals are almost formed and well separated from each other [4], and the other mechanism passes through a so-called tight transition state in which the internuclear distances among the atoms of the C-NO_2 group are shorter than in the loose one (Figure 2b). The geometries of these two types of transition states obtained in this work are given in Figure 2 and the CASSCF and CASPT2 structural parameters are collected in Table S9. It should be noted that due to the very flexible nature of the transition state given in Figure 2a, we could not find a precise stationary point; although the convergence criteria for maximum gradient and root mean square of the gradient were fulfilled, the stopping criterium for displacements was not reached.

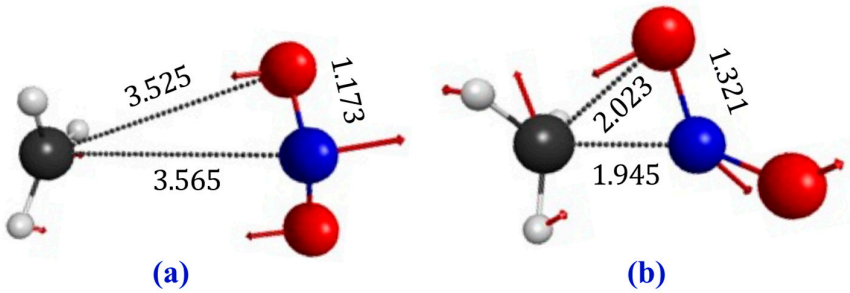

Figure 2. CASSCF/ANO-RCC optimized geometries of (**a**) loose transition state [CAS(10e,7o)] and (**b**) tight transition state [CAS(14e,11o)]. Numbers correspond to main geometrical parameters in Å; arrows: transition mode.

The loose transition state acquired a special interest in the context of the roaming reaction for the nitro–nitrite isomerization of nitromethane [7], where a nitro–nitrite isomerization mechanism which evolves through a loose transition state or roaming saddle point (RSP) is proposed. In this respect, inclusion of such an RSP seems to deviate from the original statement of the definition of roaming reaction [25], that is, a reaction that does not pass through a conventional transition state [25,27]. For this reason, we re-investigated these two types of transition states (loose and tight). To obtain such transition states, two different active spaces must be selected: (i) 10 electrons distributed in 7 orbitals for the loose transition state [CAS(10,7)], and (ii) 14 electrons in 11 orbitals [CAS(14,11)] for the tight one. The CASSCF molecular orbitals of the C_s symmetry equilibrium geometry of nitromethane, which are included in each one of the active spaces, are represented in Figure 3. The reduced active space (Figure 3a) comprises the following orbitals that coincide with the description of Saxon and Yoshimine: One O σ lone pair (n_σ), one O π lone pair (n_π), two N-O σ bonds (σ_{NO}), one N-O σ∗ bond ($\sigma*_{NO}$), one N-O π bond (π_{NO}), and one N-O π* ($\pi*_{NO}$). The larger active space (Figure 3b) comprises one O σ lone pair (n_σ), one O π lone pair (n_π), two N-O σ bonds (σ_{NO}) and the two correlating σ∗ orbitals ($\sigma*_{NO}$), one N-O π (π_{NO}) and the correlating N-O π* orbital ($\pi*_{NO}$), one C-N σ bond (σ_{CN}) and the correlating σ∗ orbital ($\sigma*_{CN}$), and the 2s orbital of nitrogen ($2s_N$) that has a strong C-N bonding character. Although both types of calculation have been performed without symmetry restrictions, the CAS(14,11) wave function of the larger active space keeps the C_s symmetry properties. In contrast, as a result of the unbalanced selection of the CAS(10,7) reduced active space, it is clearly observed in the orbitals that we obtained a symmetry breaking solution of the wave function. Symmetry breaking has an important impact on the results; generally, such results are unappropriated. For example, Figure 4 represents the 1D potential energy surfaces that connect the equilibrium geometry of nitromethane with the geometry of the loose transition state (Figure 2a), obtained with the two active spaces, CAS(10,7) and CAS(14,11), and with the linear interpolation method [68–72]. The curve obtained with the CAS(10,7) space shows a discontinuity between points 21 and 22, and the reason for this behaviour is orbital rotations (Figure 3) among the inactive, active, and secondary spaces, which, in practice, is equivalent to a change in the wave function in passing from one point to the other on the reactive domain, which is, from our point of view, chemically unacceptable to describe any reaction. Therefore, the loose transition state represented in Figure 2a must be considered an artefact of the unappropriated CAS(10,7) active space.

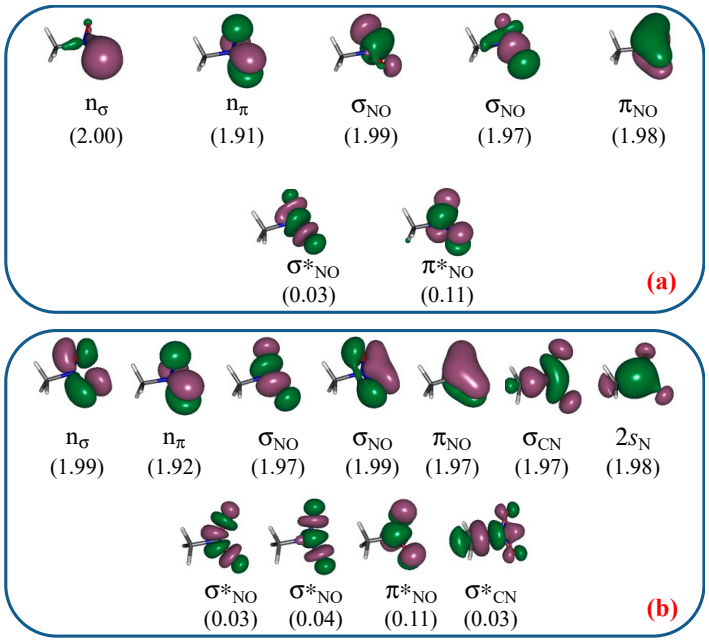

Figure 3. CASSCF/ANO-RCC molecular orbitals. (**a**) CASSCF(10e,7o); (**b**) CASSCF(14e,11o). In parenthesis: occupation numbers.

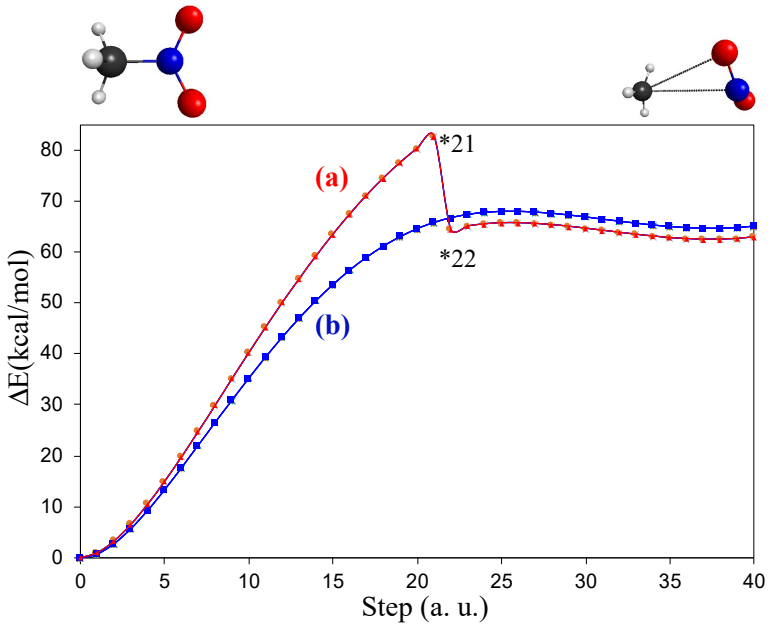

Figure 4. CASPT2 profiles of the linear interpolations in internal coordinates connecting the minimum of nitromethane (C_s) with the loose structure (C_1): (**a**) CASPT2/CASSCF(10o,7e); (**b**) CASPT2/CASSCF(14e,11o). * Indicates discontinuity in the interpolation curve due to change in the wavefunction.

Figure 5a,b depicts the 2D and 3D representations of the potential energy surfaces [CASPT2/CASSCF(14e,11o)] that comprise the configurational domain of the ternary system [CH_3NO_2:Loose:*cis*-CH_3ONO], the reference geometries that correspond to the CASPT2 minimum geometries of nitromethane and cis-methyl nitrite, plus the CASSCF loose transition state. It is clearly observed in such a figure that there is not any signal of a transition state (saddle point) which relates nitromethane with cis-methyl nitrite. In contrast, it seems that they are related through a roaming mechanism.

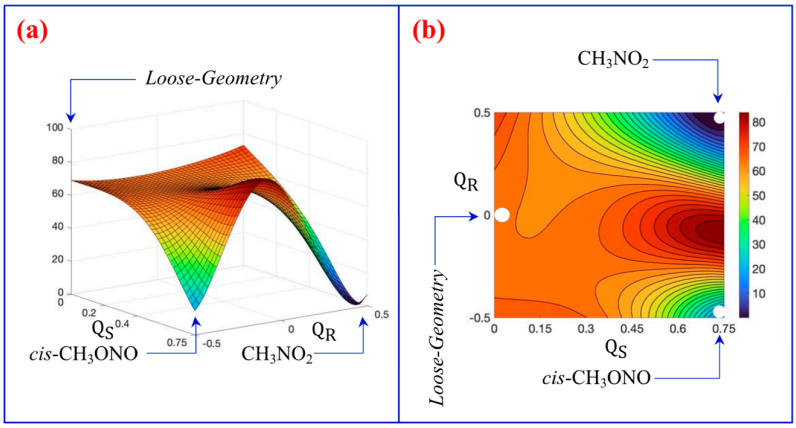

Figure 5. Mapping of the potential energy surface of the ternary system [CH_3NO_2:Loose:*cis*-CH_3ONO]; (**a**) 3D representation of potential energy and (**b**) 2D representation of potential energy. CASPT2 from CASSCF(14,11)/ANO-RCC reference wave function. Grid size (41 × 41).

To gain more insights about the roaming structures of the nitro–nitrite isomerization of nitromethane, as in Figure 5, we built four CASPT2 2D potential energy surfaces for the ternary system [CH_3NO_2-Roaming-Structure-*cis*-CH_3ONO] by taking different geometries for the quasi-dissociated species (Figure 6) and using a CASSCF(14,11) reference wave function. The first surface (Figure 6a), in fact, would not correspond to a roaming intermediate because the analysis of the wave function indicates that the two fragments are well-formed radicals; that is, the molecule is completely dissociated. The geometries and relative energies of the reference points (0_n) are included in the graphic. It is shown that a significant change in the geometry of the reference point is accompanied by a small variation in its relative energy, that is, roaming rotation must not be a very hindered process at these points of the potential energy surface, especially if rotation is assumed to be free at the higher energy geometry (0_1). Figure 6b–d represents the topology of the potential surfaces for true roaming structures. What is observed in these latter figures is that as the roaming complex is more compact with decreasing internuclear distances, the product (cis-CH_3ONO) is closer to the roaming structure; in addition, the slope of the surface becomes more negative, which enhances the formation of the intermediate [cis-CH_3ONO] from the roaming structure. To finish this paragraph, the brown flat regions on the surfaces depicted in Figure 6 correspond to very high energy points arising from geometries with very close separation between atoms.

To demonstrate that the roaming process leads to decomposition of nitromethane into CH_3O and NO passing through the methyl nitrite intermediate, we performed molecular dynamics calculations at the CASSCF level with the algorithm of Verlet [63,64]. The obtained results are shown in Figure 7. These calculations are started at the geometry represented in Figure 6c (0_3). The initial condition imposed on the dynamical calculations consists of an addition of kinetic energy on the NO_2 fragment, as is shown in Figure 7. The pattern of formation/dissociation of cis-methyl nitrite is similar in the four calculations: (i) the nitrite molecule is formed from the roaming structure, more rapid, as higher is the initial kinetic energy; (ii) the molecule lives during approximately 80 fs in the well of cis-methyl nitrite; (iii) the molecule dissociates into NO and CH_3O; and (iv) excess of kinetic energy (E_{kin} = 80 kcal/mol) leads to a delay in the dissociation process of [cis-CH_3ONO]*.

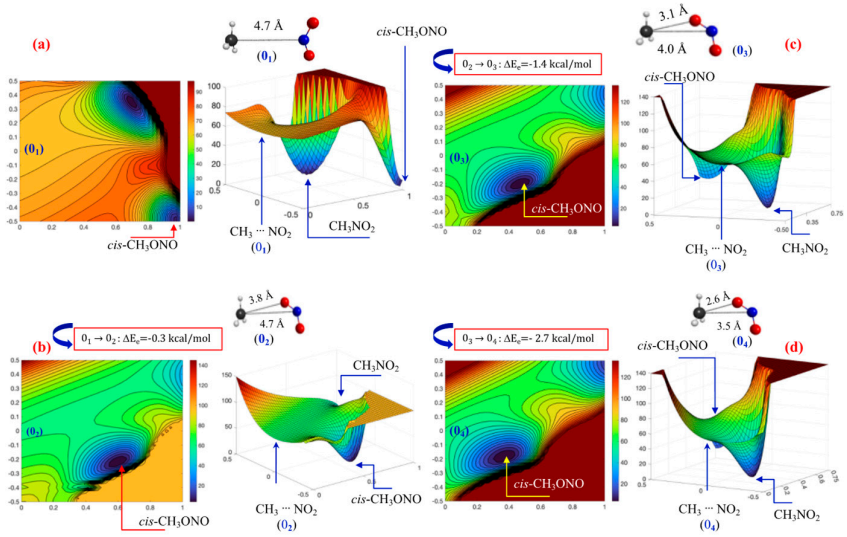

Figure 6. 2D and 3D representations of the CASPT2/CASSCF(14, 11) potential energy surfaces of the ternary system [CH_3NO_2:Roaming-Structure:*cis*-CH_3ONO] at different starting geometries 0_n. ΔE_e: electronic energy variation in passing from 0_n to 0_{n+1}. Grid size (41 × 41).

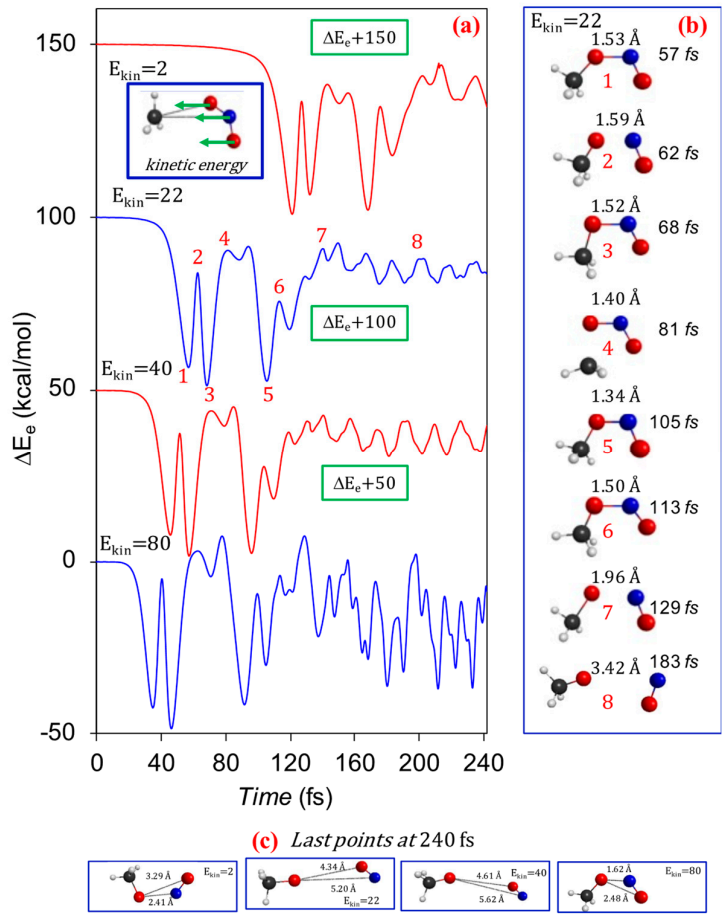

Figure 7. (**a**) CASSCF energy profiles as time function starting at the roaming geometry given in Figure 6c with different kinetic energies (inset). (**b**) Selected molecular rearrangements for the trajectory with initial condition E_{kin} = 22 kcal/mol. (**c**) End point (240 fs) in each trajectory calculation. Rectangles in (**a**) indicate displacements in *y*-axis to avoid overlapping of the curves.

The global process starting at nitromethane is represented in Equation (13):

$$CH_3NO_2 \rightarrow [CH_3 \cdots NO_2]^* \rightarrow [CH_3ONO]^* \rightarrow CH_3O + NO. \quad (13)$$

Figure 8 collects diagrammatically the Gibbs free energies at four different temperatures of the process represented in Equation (13) and Figure 6b–d. In accordance with such diagrams, the activation energy of the first step decreases as temperature increases and is the higher energy step in every case. Therefore, when the system reaches the region of the roaming rearrangement, it accumulated enough energy to complete reaction 13. Curiously, the activation energies of the process that passes through the roaming molecular arrangement with a C-N internuclear distance of 4.0 Å (Figure 6c) are the lower ones at any temperature (Figure 8b). Gibbs free energies at different temperatures have been calculated with the standard expressions of statistical thermodynamics, and the thermal corrections to the energies of the roaming structures computed after projecting out the vibrational Hessian matrix the rotation–translation eigenvectors and gradient vectors [87,88].

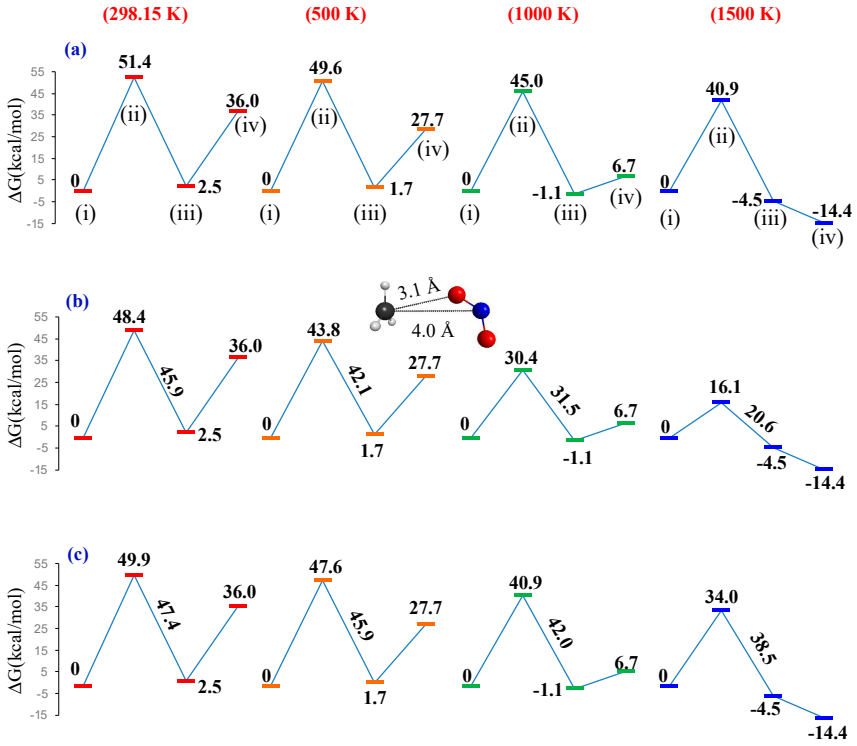

Figure 8. Schematic representation of the Gibbs energy profiles for the process (i) CH_3NO_2 → (ii) $[CH_3 \cdots NO_2]^*$ → (iii) $[CH_3ONO]^*$ → (iv) CH_3O + NO (Equation (13)) at different temperatures and initial geometries. (**a**) Initial geometry included in Figure 6b. (**b**) Initial geometry included in Figure 6c. (**c**) Initial geometry included in Figure 6d. Energetics of all the species analyzed in this figure are referred to CASPT2 electronic calculations.

4. Conclusions

In this paper is described a mapping method (orthogonalized 3D representation) for the PESs by defining an orthonormal basis consisting of two R^n orthonormal vectors that allows us to obtain a set of ordered points in the vector subspace defined by the plane that contains the basis vectors.

The main elementary unimolecular reactions of nitromethane, including energetics, geometrical optimizations, and calculated vibrational harmonic frequencies, have been studied with the CASPT2 method by using a well-balanced CASSCF reference wave function of 14(16) electrons distributed in 11(13) orbitals. All the kinetically controlled

reactions are endergonic, with the C-N bond breaking the process with lower ΔG energy among this class of reactions. In contrast, it is found that the roaming process [$CH_3NO_2 \rightarrow [CH_3 \cdots NO_2]^* \rightarrow [CH_3ONO]^* \rightarrow CH_3O + NO$] is exergonic at high temperatures, where the star symbols indicate vibrationally excited species. At this point, it is important to note that this mechanism has been previously proposed by other authors [7–9]. Furthermore, with all the roaming structures analyzed in this work, the higher energy points in the mechanism given in equation 13 are well below the dissociation limit of nitromethane that leads to CH_3 and NO_2.

The so-called loose transition state has been re-investigated with two CASSCF active spaces: (i) 10 electrons distributed in 7 orbitals and (ii) 14 electrons in 10 orbitals. It is shown that the smaller active space yields artifactual results arising from an unbalanced description of the electronic structure. In fact, the selection of the active space for studying nitromethane would be straightforward after the work of Blahous et al. on the NO_2 radical [89], where they pointed out that the CASSCF wave function to describe the whole configurational domain of the potential energy surface must contain 13 electrons distributed in 10 orbitals.

To finish, it must be remarked that an exhaustive study of a roaming process requires intensive and extensive molecular dynamics calculations, such as those performed in relevant works given in references cited above [7–10]. However, this aim is beyond the scope of this manuscript.

Supplementary Materials: The following supporting information can be downloaded at: https://www.mdpi.com/article/10.3390/reactions6010021/s1, Table S1: CASPT2 and MP2/HF geometrical parameters of nitromethane.; Table S2: Geometrical parameters of trans-methyl nitrite (trans-CH_3ONO); Table S3: Geometrical parameters of cis-methyl nitrite (cis-CH_3ONO); Table S4: Geometrical parameters of the transition state (TS1) for nitromethane to methyl-nitrite isomerization; Table S5: Geometrical parameters of the transition state (TS2) for proton migration $CH_3NO_2 \rightarrow CH_2N(O)OH$; Table S6: Geometrical parameters of the transition state (TS3) of reaction $CH_3NO_2 \rightarrow CH_2O + HNO$; Table S7: Geometrical parameters of the transition state (TS4) of reaction trans-$CH_3ONO \rightarrow$ cis-CH_3ONO; Table S8: Geometrical parameters of nitrosomethane (CH_3NO). Table S9: CASSCF and CASPT2 geometrical parameters of the loose and tight (TS1) transition states for nitromethane to methyl-nitrite isomerization. Figure S1: Orbitals and weight of the main configurations included in the CASSCF wave functions of the key geometrical structures involved in the decomposition of nitromethane. (2): doubly occupied orbital; (0) unoccupied orbital; (u) spin-up singly occupied orbital; (d) spin-down singly occupied orbital. Figure S2: MS-CASPT2 energy profiles of the linear interpolations for (a) the dissociation of CH_3NO_2 into CH_3 and NO_2; (b) the dissociation of trans-CH_3ONO into CH_3O and NO; (c) the dissociation of trans-CH_3ONO and cis-CH_3ONO into CH_3 and NO_2; Figure S3: (a) MS-CASPT2 energy profiles of the dissociation of CH_3NO_2 into CH_3NO and (O) atomic oxygen (linear interpolation in internal coordinates). Blue solid line (singlet A′); blue dotted line (singlet A″); red solid line (triplet A′); red dotted line (triplet A″). Green numbers: relative energy in kcal/mol with respect to the last point of lowest energy. (b) Calculated energetics of the isolated oxygen atom and nitrosomethane. Coordinate list: CASPT2/CASSCF/ANO-RCC Cartesian Coordinates in Å.

Funding: This research was funded by Spanish Ministry of Science and Innovation (MCIN/AEI/10.13039/501100011033) through project PID2021-122613OB-I00.

Data Availability Statement: The original contributions presented in this study are included in the article/Supplementary Materials. Further inquiries can be directed to the corresponding author.

Acknowledgments: The author thanks R. Larrosa and M. Guerrero for the technical support in running the calculations and the SCBI (Supercomputer and Bioinformatics) center of the University of Málaga (Spain) for computer resources.

Conflicts of Interest: The author declares no conflicts of interest.

References

1. Word, M.D.; Lo, H.A.; Boateng, D.A.; McPherson, S.L.; Gutsev, G.L.; Gutsev, L.G.; Lao, K.U.; Tibbetts, K.M. Ultrafast dynamics of nitro–nitrite rearrangement and dissociation in nitromethane cation. *J. Phys. Chem. A* **2022**, *126*, 879–888. [CrossRef] [PubMed]
2. Leyva, E.; Loredo-Carrillo, S.E.; Aguilar, J. Various techniques for the synthesis of 2-Nitrophenylamino-1,4-naphthoquinone derivatives. *Reactions* **2023**, *4*, 432–447. [CrossRef]
3. Zhang, J.; Peng, J.; Hu, D.; Lan, Z. Investigation of nonadiabatic dynamics in the photolysis of methyl nitrate (CH_3ONO_2) by on-the-fly surface hopping simulation. *Phys. Chem. Chem. Phys.* **2021**, *23*, 25597–25611. [CrossRef] [PubMed]
4. McKee, M.L. MCSCF study of the rearrangement of nitromethane to methyl nitrite. *J. Phys. Chem.* **1989**, *93*, 7365–7369. [CrossRef]
5. Saxon, R.P.; Yuoshimi, M. Theoretical study of nitro-nitrite rearrangement of CH_3NO_2. *Can. J. Chem.* **1992**, *70*, 572–579. [CrossRef]
6. Chang, P.; Zhou, P.; Liu, J.; Yin, S. Theoretical study on autocatalytic reaction in thermal decomposition of nitromethane. *Chem. Phys. Lett.* **2022**, *792*, 139413. [CrossRef]
7. Homayoon, Z.; Bowman, J.M. Quasiclassical trajectory study of CH_3NO_2 decomposition via roaming mediated isomerization using a global potential energy surface. *J. Phys. Chem. A* **2013**, *117*, 11665–11672. [CrossRef]
8. Zhu, R.S.; Raghunath, P.; Lin, M.C. Effect of roaming transition states upon product branching in the thermal decomposition of CH_3NO_2. *J. Phys. Chem. A* **2013**, *117*, 7308–7313. [CrossRef]
9. Zhu, R.S.; Lin, M.C. CH_3NO_2 decomposition/isomerization mechanism and product branching ratios: An ab initio chemical kinetic study. *Chem. Phys. Lett.* **2009**, *478*, 11–16. [CrossRef]
10. Isegawa, M.; Liu, F.; Maeda, S.; Morokuma, K. Ab initio reaction pathways for photodissociation and isomerization of nitromethane on four singlet potential energy surfaces with three roaming paths. *J. Chem. Phys.* **2014**, *140*, 244310. [CrossRef]
11. Arenas, J.F.; Otero, J.C.; Peláez, D.; Soto, J. Role of surface crossings in the photochemistry of nitromethane. *J. Chem. Phys.* **2005**, *122*, 084324. [CrossRef] [PubMed]
12. Arenas, J.F.; Otero, J.C.; Peláez, D.; Soto, J. The ground and excited state potential energy surfaces of nitromethane related to its dissociation dynamics after excitation at 193 nm. *J. Chem. Phys.* **2003**, *119*, 7814–7823. [CrossRef]
13. Sumida, M.; Kohge, Y.; Yamasaki, K.; Kohguchia, H. Multiple product pathways in photodissociation of nitromethane at 213 nm. *J. Chem. Phys.* **2016**, *144*, 064304. [CrossRef] [PubMed]
14. Li, W.-G.; Liu, Q.-J.; Liu, F.-S.; Liu, Z.-T. Atomic mean square displacement study of the bond breaking mechanism of energetic materials before explosive initiation. *Phys. Chem. Chem. Phys.* **2023**, *25*, 5613–5618. [CrossRef]
15. Zheng, W.; Liu, Q.-J.; Liu, F.-S.; Liu, Z.-T. Triggering the mechanism of the initial reaction of energetic materials under pressure based on Raman intensity analysis. *Phys. Chem. Chem. Phys.* **2023**, *25*, 5685–5693. [CrossRef]
16. Rice, B.M.; Sahu, S.; Owens, F.J. Density functional calculations of bond dissociation energies for NO2 scission in some nitroaromatic molecules. *J. Mol. Struct. (THEOCHEM)* **2002**, *583*, 69–72. [CrossRef]
17. Ford, J.; Seritan, S.; Zhu, X.; Sakano, M.N.; Islam, M.M.; Strachan, A.; Martínez, T.J. Nitromethane decomposition via automated reaction discovery and an ab initio corrected kinetic model. *J. Phys. Chem. A* **2021**, *125*, 1447–1460. [CrossRef]
18. Nelson, T.; Bjorgaard, J.; Greenfield, M.; Bolme, C.; Brown, K.; McGrane, S.; Scharff, R.J.; Tretiak, S. Ultrafast photodissociation dynamics of nitromethane. *J. Phys. Chem. A* **2016**, *120*, 519–526. [CrossRef]
19. Dey, A.; Fernando, R.; Abeysekera, C.; Homayoon, Z.; Bowman, J.M.; Suits, A.G. Photodissociation dynamics of nitromethane and methyl nitrite by infrared multiphoton dissociation imaging with quasiclassical trajectory calculations: Signatures of the roaming pathway. *J. Chem. Phys.* **2014**, *140*, 054305. [CrossRef]
20. Annesley, C.J.; Randazzo, J.B.; Klippenstein, S.J.; Harding, L.B.; Jasper, A.W.; Georgievskii, Y.; Ruscic, B.; Tranter, R.S. Thermal dissociation and roaming isomerization of nitromethane: Experiment and theory. *J. Phys. Chem. A* **2015**, *119*, 7872–7893. [CrossRef]
21. Wodtke, A.M.; Hintsa, E.J.; Lee, Y.T. Infrared Multiphoton Dissociation of Three Nitroalkanes. *J. Phys. Chem.* **1986**, *90*, 3549–3558. [CrossRef]
22. Bhattacharya, A.; Guo, Y.Q.; Bernstein, E.R. A comparison of the decomposition of electronically excited nitro-containing molecules with energetic moieties C-NO_2, N-NO_2, and O-NO_2. *J. Chem. Phys.* **2012**, *136*, 024321. [CrossRef] [PubMed]
23. Guo, Y.Q.; Bhattacharya, A.; Bernstein, E.R. Photodissociation dynamics of nitromethane at 226 and 271 nm at both nanosecond and femtosecond time scales. *J. Phys. Chem. A* **2009**, *113*, 85–96. [CrossRef] [PubMed]
24. Matsugi, A.; Shiina, H. Thermal decomposition of nitromethane and reaction between CH_3 and NO_2. *J. Phys. Chem. A* **2017**, *121*, 4218–4224. [CrossRef]
25. Townsend, D.; Lahankar, S.A.; Lee, S.K.; Chambreau, S.D.; Suits, A.G.; Zhang, X.; Rheinecker, J.; Harding, L.B.; Bowman, J.M. The roaming atom: Straying from the reaction path in formaldehyde decomposition. *Science* **2004**, *306*, 1158–1161. [CrossRef]
26. Herath, N.; Suits, A.G. Roaming radical reactions. *J. Phys. Chem. Lett.* **2011**, *2*, 642–647. [CrossRef]
27. Suits, A.G. Roaming reactions and dynamics in the van der Waals region. *Annu. Rev. Phys. Chem.* **2020**, *71*, 77–100. [CrossRef]

28. Lopez, J.G.; Vayner, G.; Lourderaj, U.; Addepalli, S.V.; Kato, S.; Dejong, W.A.; Windus, T.L.; Hase, W.L. A direct dynamics trajectory study of F^-+CH_3OOH reactive collisions reveals a major non-IRC reaction path. *J. Am. Chem. Soc.* **2007**, *129*, 9976–9985. [CrossRef]
29. Pomerantz, A.E.; Camden, J.P.; Chiou, A.S.; Ausfelder, F.; Chawla, N.; Hase, W.L.; Zare, R.N. Reaction products with internal energy beyond the kinematic limit result from trajectories far from the minimum energy path: An example from H + HBr → H_2 + Br. *J. Am. Chem. Soc.* **2005**, *127*, 16368–16369. [CrossRef]
30. Lourderaj, U.; Park, K.; Hase, W.L. Classical trajectory simulations of post-transition state dynamics. *Int. Rev. Phys. Chem.* **2008**, *27*, 361–403. [CrossRef]
31. Suits, A.G. Roaming atoms and radicals: A new mechanism in molecular dissociation. *Acc. Chem. Res.* **2008**, *41*, 873–881. [CrossRef] [PubMed]
32. Bowman, J.M.; Shepler, B.C. Roaming radicals. *Annu. Rev. Phys. Chem.* **2011**, *62*, 531–553. [CrossRef] [PubMed]
33. Bowman, J.M.; Houston, P.L. Theories and simulations of roaming. *Chem. Soc. Rev.* **2017**, *46*, 7615–7624. [CrossRef] [PubMed]
34. Houston, P.L.; Kable, S.H. Photodissociation of acetaldehyde as a second example of the roaming mechanism. *Proc. Natl. Acad. Sci. USA* **2006**, *103*, 16079–16082. [CrossRef]
35. Harding, L.B.; Klippenstein, S.J.; Jasper, A.W. Ab initio methods for reactive potential surfaces. *Phys. Chem. Chem. Phys.* **2007**, *9*, 4055–4070. [CrossRef]
36. Heazlewood, B.R.; Jordan, M.J.T.; Kable, S.H.; Selby, T.M.; Osborn, D.L.; Shepler, B.C.; Braams, B.J.; Bowman, J.M. Roaming is the dominant mechanism for molecular products in acetaldehyde photodissociation. *Proc. Natl. Acad. Sci. USA* **2008**, *105*, 12719–12724. [CrossRef]
37. Roos, B.O. The Complete Active Space Self-Consistent Field Method and Its Applications in Electronic Structure Calculations. In *Advances in Chemical Physics*; Ab initio Methods in Quantum Chemistry II; Lawley, K.P., Ed.; John Wiley & Sons: Chichester, UK, 1987; Chapter 69; p. 399.
38. Roos, B.O.; Taylor, P.R.; Siegbahn, P.E.M. A complete active space SCF method (CASSCF) using a density matrix formulated super-CI approach. *Chem. Phys.* **1980**, *48*, 157–173. [CrossRef]
39. Roos, B.O. The complete active space scf method in a Fock-matrix-based super-CI formulation. *Int. J. Quantum Chem.* **1980**, *18*, 175–189. [CrossRef]
40. Siegbahn, P.E.M.; Almlo, J.; Heiberg, A.; Roos, B.O. The complete active space scf (CASSCF) method in a Newton-Raphson formulation with application to the HNO molecule. *J. Chem. Phys.* **1981**, *74*, 2384–2396. [CrossRef]
41. Werner, H.-J.; Meyer, W. A quadratically convergent multiconfiguration-self-consistent field method with simultaneous-optimization of orbitals and cl coefficients. *J. Chem. Phys.* **1980**, *73*, 2342–2356. [CrossRef]
42. Werner, H.-J.; Meyer, W. A quadratically convergent MCSCF method for the simultaneous-optimization of several states. *J. Chem. Phys.* **1981**, *74*, 5794–5801. [CrossRef]
43. Olsen, J. The CASSCF method: A perspective and commentary. *Int. J. Quantum. Chem.* **2011**, *111*, 3267–3272. [CrossRef]
44. Roos, B.O.; Andersson, K.; Fu, M.P.; Malmqvist, P.Â.; Serrano-Andre, L.; Pierloot, K.; Mercha, M. Multiconfigurational perturbation theory: Applications in electronic spectroscopy. *Adv. Chem. Phys.* **1996**, *93*, 219–331.
45. Finley, J.; Malmqvist, P.-Å.; Roos, B.O.; Serrano-Andrés, L. The multi-state CASPT2 method. *Chem. Phys. Lett.* **1998**, *288*, 299–306. [CrossRef]
46. Veryazov, V.; Widmark, P.O.; Serrano-Andrés, L.; Lindh, R.; Roos, B.O. 2MOLCAS as a development platform for quantum chemistry software. *Int. J. Quantum Chem.* **2004**, *100*, 626–635. [CrossRef]
47. Aquilante, F.; Autschbach, J.; Carlson, R.K.; Chibotaru, L.F.; Delcey, M.G.; De Vico, L.; Fdez. Galván, I.; Ferré, N.; Frutos, L.M.; Gagliardi, L. Molcas 8: New capabilities for multiconfigurational quantum chemical calculations across the periodic table. *J. Comp. Chem.* **2016**, *37*, 506–541. [CrossRef]
48. Fdez Galván, I.; Vacher, M.; Alavi, A.; Angeli, C.; Aquilante, F.; Autschbach, J.; Bao, J.J.; Bokarev, S.I.; Bogdanov, N.A.; Carlson, R.K.; et al. OpenMolcas: From Source Code to Insight. *J. Chem. Theory Comput.* **2019**, *15*, 5925–5964. [CrossRef]
49. Aquilante, F.; Autschbach, J.; Baiardi, A.; Battaglia, S.; Borin, V.A.; Chibotaru, L.F.; Conti, I.; De Vico, L.; Delcey, M.; Ferré, N.; et al. Modern quantum chemistry with [Open] Molcas. *J. Chem. Phys.* **2020**, *152*, 214117. [CrossRef]
50. Roos, B.O.; Lindh, R.; Malmqvist, P.-Å.; Veryazov, V.; Widmark, P.-O. Main group atoms and dimers studied with a new relativistic ANO basis set. *J. Phys. Chem. A* **2004**, *108*, 2851–2858. [CrossRef]
51. Roos, B.O.; Lindh, R.; Malmqvist, P.-Å.; Veryazov, V.; Widmark, P.-O. New relativistic ANO basis sets for transition metal atoms. *J. Phys. Chem. A* **2005**, *109*, 6575–6579. [CrossRef]
52. Møller, C.; Plesset, M.S. Note on an approximation treatment for many-electron systems. *Phys. Rev.* **1934**, *46*, 618–622. [CrossRef]
53. Zhao, Y.; Truhlar, D.G. The M06 suite of density functionals for main group thermochemistry, thermochemical kinetics, noncovalent interactions, excited states, and transition elements: Two new functionals and systematic testing of four M06-class functionals and 12 other functionals. *Theor. Chem. Acc.* **2008**, *120*, 215–241.

54. Frisch, M.E.; Trucks, G.W.; Schlegel, H.B.; Scuseria, G.E.; Robb, M.; Cheeseman, J.R.; Scalmani, G.; Barone, V.P.G.A.; Petersson, G.A.; Nakatsuji, H.J.R.A.; et al. *Gaussian 16, Revision C.02*; Gaussian, Inc.: Wallingford, CT, USA, 2016.
55. Weigend, F.; Ahlrichs, R. Balanced basis sets of split valence, triple zeta valence and quadruple zeta valence quality for H to Rn: Design and assessment of accuracy. *Phys. Chem. Chem. Phys.* **2005**, *7*, 3297–3305. [CrossRef]
56. Weigend, F. Accurate Coulomb-fitting basis sets for H to Rn. *Phys. Chem. Chem. Phys.* **2006**, *8*, 1057–1065. [CrossRef]
57. Soto, J.; Algarra, M. Electronic structure of nitrobenzene: A benchmark example of the accuracy of the multi-state CASPT2 theory. *J. Phys. Chem. A* **2021**, *125*, 9431–9437. [CrossRef] [PubMed]
58. Arenas, J.F.; Otero, J.C.; Peláez, D.; Soto, J.; Serrano-Andrés, L. Multiconfigurational second-order perturbation study of the decomposition of the radical anion of nitromethane. *J. Chem. Phys.* **2004**, *121*, 4127–4132. [CrossRef]
59. Arenas, J.F.; Otero, J.C.; Peláez, D.; Soto, J. Photodissociation mechanism of nitramide: A CAS-SCF and MS-CASPT2 study. *J. Phys. Chem. A* **2005**, *109*, 7172–7180. [CrossRef]
60. Soto, J.; Peláez, D.; Otero, J.C.; Avila, F.J.; Arenas, J.F. Photodissociation mechanism of methyl nitrate. A study with the multistate second-order multiconfigurational perturbation theory. *Phys. Chem. Chem. Phys.* **2009**, *11*, 2631–2639. [CrossRef]
61. Zhang, J.J.; Peng, J.W.; Zhu, Y.F.; Hu, D.P.; Lan, Z.G. Influence of mode-specific excitation on the nonadiabatic dynamics of methyl nitrate (CH_3ONO_2). *J. Phys. Chem. Lett.* **2023**, *14*, 6542–6549. [CrossRef]
62. Zhang, J.J.; Peng, J.W.; Hu, D.P.; Xu, C.; Lan, Z.G. Understanding photolysis of CH_3ONO_2 with on-the-fly nonadiabatic dynamics simulation at the ADC(2) Level. *Chin. J. Chem. Phys.* **2022**, *35*, 451–460. [CrossRef]
63. Verlet, L. Computer experiments on classical fluids. I. Thermodynamical properties of Lennard-Jones molecules. *Phys. Rev.* **1967**, *159*, 98–103. [CrossRef]
64. Swope, W.C.; Andersen, H.C.; Berens, P.H.; Wilson, K.R. A computer-simulation method for the calculation of equilibrium-constants for the formation of physical clusters of molecules-application to small water clusters. *J. Chem. Phys.* **1982**, *76*, 637–649. [CrossRef]
65. Schaftenaar, G.; Noordik, J.H. Molden: A pre- and post-processing program for molecular and electronic structures. *J. Comput. Aided Mol. Des.* **2000**, *14*, 123–134. [CrossRef] [PubMed]
66. Allouche, A.R. Gabedit-a graphical user interface for computational chemistry softwares. *J. Comput. Chem.* **2011**, *32*, 174–182. [CrossRef]
67. BBode, M.; Gordon, M.S. MacMolPlt: A graphical user interface for GAMESS. *J. Mol. Graphics Modell.* **1998**, *16*, 133–138. [CrossRef]
68. Soto, J.; Peláez, D.; Algarra, M. CASPT2 study of the electronic structure and photochemistry of protonated N-nitrosodimethylamine (NDMA-H+) at 453 nm. *J. Chem. Phys.* **2023**, *158*, 204301. [CrossRef]
69. Aranda, D.; Avila, F.J.; López-Tocón, I.; Arenas, J.F.; Otero, J.C.; Soto, J. An MS-CASPT2 study of the photodecomposition of 4-methoxyphenyl azide: Role of internal conversion and intersystem crossing. *Phys. Chem. Chem. Phys.* **2018**, *20*, 7764–7771. [CrossRef]
70. Soto, J.; Otero, J.C.; Avila, F.J.; Peláez, D. Conical intersections and intersystem crossings explain product formation in photochemical reactions of aryl azides. *Phys. Chem. Chem. Phys.* **2019**, *21*, 2389–2396. [CrossRef]
71. Soto, J. Photochemistry of 1-phenyl-1-diazopropane and its Diazirine isomer: A CASSCF and MS-CASPT2 study. *J. Phys. Chem. A* **2022**, *126*, 8372–8379. [CrossRef]
72. Peláez, D.; Arenas, J.F.; Otero, J.C.; Soto, J. A complete active space self-consistent field study of the photochemistry of nitrosamine. *J. Chem. Phys.* **2006**, *125*, 164311. [CrossRef]
73. Soto, J.; Arenas, J.F.; Otero, J.C.; Peláez, D. Effect of an S1/S0 conical intersection on the chemistry of nitramide in its ground state. A comparative CASPT2 study of the nitro-nitrite isomerization reactions in nitramide and nitromethane. *J. Phys. Chem. A* **2006**, *110*, 8221–8226. [CrossRef] [PubMed]
74. Arenas, J.F.; Centeno, S.P.; López-Tocón, I.; Peláez, D.; Soto, J. DFT and CASPT2 study of two thermal reactions of nitromethane: C-N bond cleavage and nitro-to-nitrite isomerization. An example of the inverse symmetry breaking deficiency in density functional calculations of an homolytic dissociation. *J. Mol. Struct. (THEOCHEM)* **2003**, *630*, 17–23. [CrossRef]
75. Ruscic, B.; Pinzon, R.E.; Morton, M.L.; von Laszevski, G.; Bittner, S.J.; Nijsure, S.G.; Amin, K.A.; Minkoff, M.; Wagner, A.F. Introduction to active thermochemical tables: Several "key" enthalpies of formation revisited. *J. Phys. Chem. A* **2004**, *108*, 9979–9997. [CrossRef]
76. Ruscic, B.; Pinzon, R.E.; von Laszewski, G.; Kodeboyina, D.; Burcat, A.; Leahy, D.; Montoy, D.; Wagner, A.F. Active Thermochemical Tables: Thermochemistry for the 21st century. *J. Phys. Conf. Ser.* **2005**, *16*, 561–570. [CrossRef]
77. Ruscic, B.; Bross, D.H. Active Thermochemical Tables (ATcT), Values Based on Ver. 1.124 of the Thermochemical Network. 2022. Available online: https://atct.anl.gov/Thermochemical%20Data/version%201.124/index.php (accessed on 7 March 2025).
78. Cox, A.P.; Waring, S. Microwave-spectrum and structure of nitromethane. *J. Chem. Soc. Faraday Trans. II* **1972**, *68*, 1060–1071. [CrossRef]
79. Turner, P.H.; Corkill, M.J.; Cox, A.P. Microwave-spectra and structures of cis-methyl nitrite and trans-methyl nitrite-methyl barrier in trans-methyl nitrite. *J. Phys. Chem.* **1979**, *83*, 1473–1482. [CrossRef]

80. Van der Veken, B.J.; Maas, R.; Guirgis, G.A.; Stidham, G.A.; Sheehan, T.G.; Durig, J.R. Infrared spectrum, ab initio calculations, barriers to internal-rotation, and structural parameters for methyl nitrite. *J. Phys. Chem.* **1990**, *94*, 4029–4039. [CrossRef]
81. Turner, P.H.; Cox, A.P. Dipole Moment of Acetaldehyde. Microwave-spectrum, structure, dipole-moment and centrifugal-distortion of nitrosomethane-dipole-moment of acetaldehyde. *J. Chem. Soc. Faraday Trans. II* **1978**, *74*, 533–559. [CrossRef]
82. Soto, J. Identification of the photoreactive species of protonated N-nitrosopiperidine in acid medium: A CASPT2 and DFT study. *J. Phys. Chem. A* **2023**, *127*, 9781–9786. [CrossRef]
83. Soto, J.; Peláez, D.; Otero, J.C. A SA-CASSCF and MS-CASPT2 study on the electronic structure of nitrosobenzene and its relation to its dissociation dynamics. *J. Chem. Phys.* **2021**, *154*, 044307. [CrossRef]
84. Liu, M.K.; Li, J.; Li, Q.S.; Li, Z.S. Theoretical insights into photo-induced isomerization mechanisms of phenylsulfinyl radical PhSO˙. *Phys. Chem. Chem. Phys.* **2022**, *24*, 6266–6273. [CrossRef] [PubMed]
85. Mu, D.; Li, Q.S. A theoretical study on the photochemical generation of phenylborylene from phenyldiazidoborane. *Phys. Chem. Chem. Phys.* **2023**, *25*, 8074–8081. [CrossRef] [PubMed]
86. Peng, X.L.; Migani, A.; Li, Q.S.; Li, Z.S.; Blancafort, L. Theoretical study of non-Hammett vs. Hammett behaviour in the thermolysis and photolysis of arylchlorodiazirines. *Phys. Chem. Chem. Phys.* **2018**, *20*, 1181–1188. [CrossRef]
87. Soto, J.; Algarra, M.; Peláez, D. Nitrene formation is the first step of the thermal and photochemical decomposition reactions of organic azides. *Phys. Chem. Chem. Phys.* **2022**, *24*, 5109–5115. [CrossRef]
88. Arenas, J.F.; Marcos, J.I.; López-Tocón, I.; Otero, J.C.; Soto, J. Potential-energy surfaces related to the thermal decomposition of ethyl azide: The role of intersystem crossings. *J. Chem. Phys.* **2000**, *113*, 2282–2289. [CrossRef]
89. Blahous, C.P., III; Yates, B.F.; Xie, Y.; Schaefer, H.F., III. Symmetry-breaking in the NO_2 sigma-radical-construction of the 2A1-state and 2B2-state with Cs symmetry complete active space self-consistent-field wave-functions. *J. Chem. Phys.* **1990**, *93*, 8105–8109. [CrossRef]